THE JOURNAL OF BIOLOGICAL CHEMISTRY VOL. 283, NO. 27, pp. 19132–19139, July 4, 2008

Structural and Biochemical Basis for the Binding Selectivity of Peroxisome Proliferator-activated Receptor γ to PGC-1α*

Received for publication, March 13, 2008, and in revised form, May 8, 2008 Published, JBC Papers in Press, May 9, 2008, DOI 10.1074/jbc.M802040200

Yong Li[‡§1], **Amanda Kovach**[‡], **Kelly Suino-Powell**[‡], **Dariusz Martynowski**[§], **and H. Eric Xu**[‡2]

From the [‡]*Laboratory of Structural Sciences, Van Andel Research Institute, Grand Rapids, Michigan 49503 and the* [§]*Department of Pharmaceutical Sciences, Center for Pharmacogenetics, University of Pittsburgh, Pittsburgh, Pennsylvania 15261*

The functional interaction between the peroxisome proliferator-activated receptor γ (PPARγ) and its coactivator PGC-1α is crucial for the normal physiology of PPARγ and its pharmacological response to antidiabetic treatment with rosiglitazone. Here we report the crystal structure of the PPARγ ligand-binding domain bound to rosiglitazone and to a large PGC-1α fragment that contains two LXXLL-related motifs. The structure reveals critical contacts mediated through the first LXXLL motif of PGC-1α and the PPARγ coactivator binding site. Through a combination of biochemical and structural studies, we demonstrate that the first LXXLL motif is the most potent among all nuclear receptor coactivator motifs tested, and only this motif of the two LXXLL-related motifs in PGC-1α is capable of binding to PPARγ. Our studies reveal that the strong interaction of PGC-1α and PPARγ is mediated through both hydrophobic and specific polar interactions. Mutations within the context of the full-length PGC-1α indicate that the first PGC-1α motif is necessary and sufficient for PGC-1α to coactivate PPARγ in the presence or absence of rosiglitazone. These results provide a molecular basis for specific recruitment and functional interplay between PPARγ and PGC-1α in glucose homeostasis and adipocyte differentiation.

Peroxisome proliferator-activated receptor γ (PPARγ)[3] and its two related receptors, PPARα and β/δ, comprise a subfamily of ligand-regulated nuclear receptors involved in many aspects of human physiology. PPARγ is a key regulator involved in adipocyte differentiation, glucose homeostasis, and inflammatory responses (1, 2). PPARγ also is the molecular target of pioglitazone (Actos) and rosiglitazone (Avandia), a class of thiazolidinedione drugs used for treating type 2 diabetes patients. These drugs improve insulin sensitivity and increase glucose and fatty acid metabolism. PPARγ ligands may also have application in the treatment of inflammation and cancer (3, 4). However, the clinical use of PPARγ ligands is clearly tempered by side effects such as edema, weight gain, and increased incidence of heart attack. The undesired side effects of thiazolidinedione drugs are possibly associated with the cross-reactivity of these ligands with two other PPARs because of low selectivity and/or the inherent PPARγ activation because of multiple functions of PPARγ (5, 6).

The pharmacological actions of rosiglitazone are mediated through the PPAR ligand-binding domain (LBD), which binds ligands and then recruits nuclear receptor coactivators (or corepressors) to regulate the expression of downstream target genes. Currently there are ~300 nuclear receptor coregulators, including the steroid receptor coactivators (SRC) 1, 2, and 3 and the nuclear corepressors N-CoR and SMRT (7, 8). The functional profile of PPARγ in response to ligand binding is largely determined by the selective use of transcriptional coregulators because ligand-specific recruitment of coregulators ultimately controls the transcriptional output of the target genes. Thus, ligand-bound PPARγ may show diverse pharmacological functions depending on the specific binding of coactivators. Analogous to many other nuclear receptors, the ligand-dependent recruitment of coactivators by PPARγ is primarily determined by the interaction of coactivator LXXLL motifs with the receptor LBD. Crystal structures of various LBD·coactivator complexes reveal a conserved binding mode for coactivator LXXLL motifs by nuclear receptors (9, 10). Upon the binding of an agonist, nuclear receptors use a charge-clamp pocket, in part composed of the C-terminal activation function 2 helix, to form a hydrophobic groove for binding the LXXLL motif of the coactivators. However, there are numerous coactivators with distinct functions, each containing multiple LXXLL motifs. The precise mechanism for recruitment of specific coactivators by PPARγ remains poorly defined.

The PPARγ coactivator 1α (PGC-1α) is a nuclear coactivator that interacts with many transcription factors, including most members of the nuclear hormone receptor family. PGC-1α was originally identified as a coactivator that interacts with PPARγ in a ligand-independent manner (11). Besides PPARγ, PGC-1α is also able to coactivate a number of other nuclear receptors through conserved LXXLL motifs, including glucocorticoid

* This work was supported, in whole or in part, by National Institutes of Health Grants DK071662 and DK066202 (to H. E. X.) and HL089301 (to H. E. X. and Y. L.). This work was also supported by a grant from the Jay and Betty Van Andel Foundation (to H. E. X.), a grant from the Competitive Medical Research Fund of The University of Pittsburgh Medical Center Health System (to Y. L.), and an award from the American Heart Association (to Y. L.). Use of the Advanced Photon Source was supported by the Office of Science of the United States Department of Energy. The costs of publication of this article were defrayed in part by the payment of page charges. This article must therefore be hereby marked "*advertisement*" in accordance with 18 U.S.C. Section 1734 solely to indicate this fact.

The atomic coordinates and structure factors (code 3CS8) have been deposited in the Protein Data Bank, Research Collaboratory for Structural Bioinformatics, Rutgers University, New Brunswick, NJ (http://www.rcsb.org/).

[1] To whom correspondence may be addressed: 709 Salk Hall, Pittsburgh, PA 15261. Fax: 412-648-1664; E-mail: yol21@pitt.edu.

[2] To whom correspondence may be addressed: 333 Bostwick Ave., Grand Rapids, MI 49503. Fax: 616-234-5773; E-mail: eric.xu@vai.org.

[3] The abbreviations used are: PPARγ, peroxisome proliferator-activated receptor γ; SRC, steroid receptor coactivator; PGC-1α, PPARγ coactivator 1α; LBD, ligand-binding domain; MOPS, 4-morpholinepropanesulfonic acid; CHAPS, 3-[(3-cholamidopropyl)dimethylammonio]-1-propanesulfonic acid; ERRα, estrogen-related receptor α.

receptor, PPARα, estrogen receptor, and estrogen-related receptor α (ERRα) (12–16). PGC-1α is expressed in brown adipose tissue, brain, heart, kidney, and cold-exposed skeletal muscle (17). In white adipose tissue, the expression of PGC-1α is substantially increased by treatment with the thiazolidinedione rosiglitazone, suggesting the importance of PGC-1α in rosiglitazone-regulated PPARγ activity (18). Mapping of PGC-1α defined one nuclear receptor interaction domain with a consensus L*XX*LL motif (residues 144–148, ID1) and an LLKYL motif (residues 210–214, ID2) that are important for binding nuclear receptors. For example, both biochemical data and the crystal structure of the ERRα LBD bound to the PGC-1α LLKYL motif (ID2) reveal the specific binding of this inverted leucine-rich motif to ERRα (15, 19). However, the molecular basis for the interaction between PPARγ and PGC-1α remains unclear.

To investigate the molecular mechanisms of rosiglitazone-regulated PPARγ activity, we first determined the preferred coactivator motifs for PPARγ in response to rosiglitazone using biochemical peptide profiling. Among the coactivator motifs tested, the PGC-1α ID1 motif was shown to have the highest binding affinity to PPARγ. To uncover the molecular mechanism for the binding selectivity of PPARγ to PGC-1α, we went on to solve the crystal structure of the PPARγ LBD bound to a large fragment of PGC-1α containing both ID1 and ID2 L*XX*LL-related motifs. The structure revealed that only ID1 is capable of binding to PPARγ. Mutations within the context of the full-length PGC-1α indicate that the first PGC-1α motif is necessary and sufficient for PGC-1α to coactivate PPARγ in the presence or absence of rosiglitazone. These results provide a structural and biochemical basis for specific recruitment of PGC-1α by the rosiglitazone-bound PPARγ.

EXPERIMENTAL PROCEDURES

Protein Preparation—Both the human PPARγ LBD (residues 206–477) and the human PGC-1α fragment (residues 101–220), each containing a His_6 tag, were expressed from the expression vector pETDuet1 (Novagen). BL21(DE3) cells transformed with this expression plasmid were grown in LB broth at 25 °C to an A_{600} of 1 and induced with 0.1 mM isopropyl 1-thio-β-D-galactopyranoside at 16 °C. Cells were harvested, resuspended in 400 ml of extract buffer (50 mM Tris, pH 8.0, 150 mM NaCl, 10% glycerol, and 25 mM imidazole) per 12 liters of cells, and passed three times through a French press with pressure set at 1000 pascals. The lysate was centrifuged at 20,000 rpm for 30 min, and the supernatant was loaded onto a nickel-nitrilotriacetic acid column. The column was washed with extract buffer, and the protein was eluted with a 300-ml gradient to the buffer (10 mM Tris, pH 8.0, 150 mM NaCl, 10% glycerol, and 500 mM imidazole). Both human PPARγ LBD and the PGC-1α fragment were further purified on a Q-Sepharose column. The purified PPARγ and the PGC-1α fragment that contains both L*XX*LL motifs were mixed at a ratio of 1:2 with a 5-fold excess of the PPARγ ligand rosiglitazone. The ternary complex was further purified by gel filtration (20 mM Tris, pH 8.0, 100 mM NaCl, and 5 mM DTT) and filter-concentrated to 10 mg/ml.

Crystallization, Data Collection, Structure Determination, and Refinement—The PPARγ·rosiglitazone·PGC-1α crystals were grown at room temperature in hanging drops containing 1.0 μl of the above protein solution and 1.0 μl of well solution containing 0.2 M ammonium iodide (pH 6.2) and 20% polyethylene glycol 3350. The crystals were directly frozen in liquid nitrogen for data collection. The PPARγ·rosiglitazone·PGC-1α crystals formed in the C2 space group, with $a = 95.11$, $b = 53.89$, and $c = 64.89$ Å, $\alpha = \beta = 90°$, and $\gamma = 105°$, and contained one molecule/crystallographic asymmetric unit. A full 360° of data were collected from a single crystal using 1° oscillation by a MAR165 CCD detector at the ID line of sector 32 of the Advanced Photon Source. The observed reflections were reduced, merged, and scaled with the HKL2000 package (20). The structures were determined with the AmoRe program by molecular replacement using the crystal structure of PPARγ LBD (21) as a model (22). Manual model building was carried out with QUANTA (Accelrys, Inc.), and structure refinement was proceeded with crystallography NMR software (23).

AlphaScreen Binding Assays—The binding of various peptide motifs to PPARγ was determined by AlphaScreen assays using a hexahistidine detection kit from PerkinElmer Life Sciences, as described recently for other nuclear receptors (24, 25). The experiments were conducted with ~20 nM His tag receptor LBD and 20 nM biotinylated SRC2-3 peptide or other coactivator peptides in the presence of 5 μg/ml donor and acceptor beads in a buffer containing 50 nM MOPS, 50 mM NaF, 50 mM CHAPS, and 0.1 mg/ml bovine serum albumin, all adjusted to pH 7.4. The biotinylated peptides used in Fig. 1*A* are as follows: SRC2-3 (TIF2), QEPVSPKKKENALLRYLLDKDDTKD; SRC1-2, SPSSHSSLTERHKILHRLLQEGSP; SRC1-4, QKPTSGPQTPQAQQKSLLQQLLTE; PGC-1α-1, AEEPSLLKKLLLAPA; CBP-1, SGNLVPDAASKHKQLSELLRGGSG; and TRAP, GHGEDFSKVSQNPILTSLLQITGN.

The relative binding affinity of peptide L*XX*LL motifs was determined using unlabeled peptides at 500 nM to compete with the binding of biotinylated SRC2-3 to PPARγ LBD. The sequences of unlabeled peptides used in Fig. 1*B* are as before (26). IC_{50} values for various coactivator L*XX*LL motifs were determined from a nonlinear least squares fit of the data based on an average of three repeated experiments from the dose-response curves.

Transient Transfection Assays—COS-7 cells were maintained in Dulbecco's modified Eagle's medium containing 10% fetal bovine serum and were transiently transfected using Lipofectamine 2000 (Invitrogen). Twenty-four-well plates were plated 24 h prior to transfection (5×10^4 cells/well). For mammalian two-hybrid assays, cells were transfected with 200 ng of Gal4-PGC-1α (residues 101–220), 200 ng of VP16-PPARγ LBD (residues 206–477), and 200 ng of pG5Luc (Promega). For full-length PPARγ reporter assays, the cells were transfected with plasmids encoding full-length PPARγ, coactivators, and PPRE-luciferase. Eighteen h after transfection, ligands were added in Dulbecco's modified Eagle's medium supplemented with 5% charcoal/dextran-treated fetal bovine serum (Hyclone). Cells were harvested 24 h later for luciferase assays. Luciferase data were normalized to *Renilla* activity as an internal control.

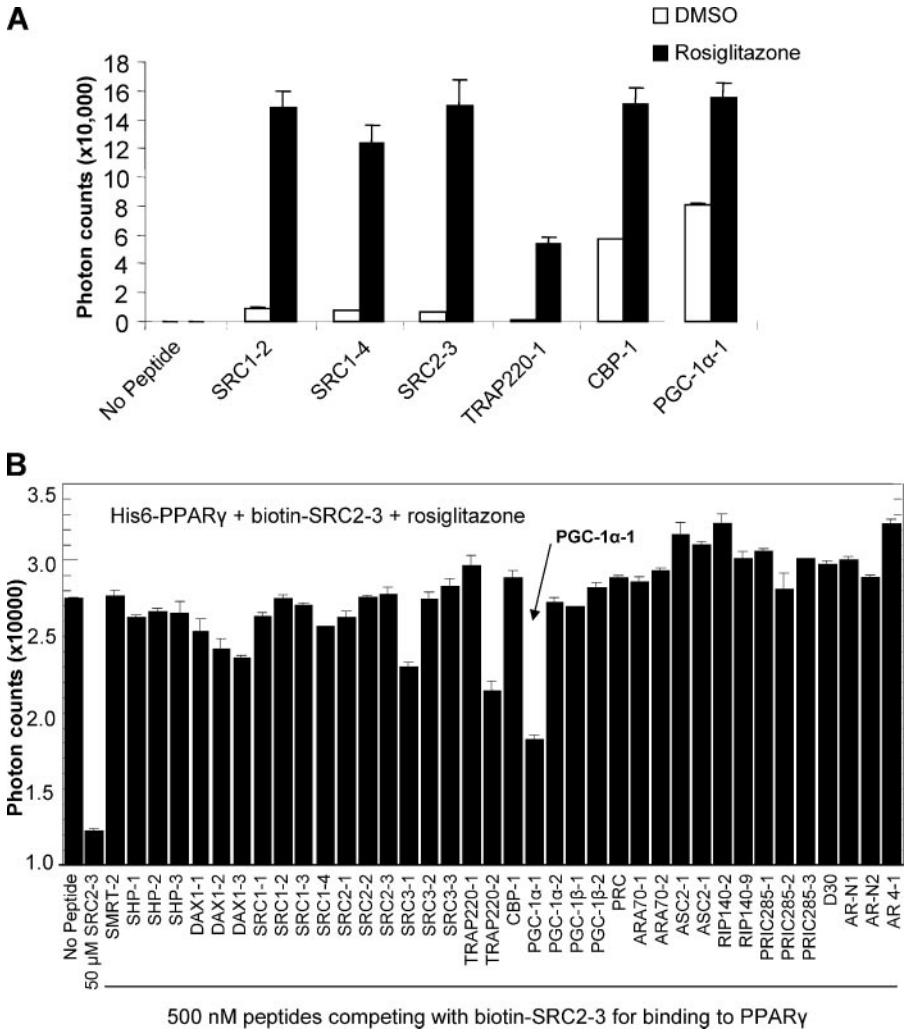

FIGURE 1. **PGC-1α has a high binding affinity for PPARγ LBD in response to rosiglitazone.** *A*, ligand-dependent binding of various coactivator L*XX*LL motifs to the PPARγ LBD by AlphaScreen assays. Background reading with the PPARγ LBD is <200 photons. *DMSO*, dimethyl sulfoxide. *B*, relative binding affinity of various coregulator peptide motifs to the PPARγ LBD in the presence of rosiglitazone is determined by peptide competition. Various unlabeled peptides (500 nM) are used to compete with the binding of the biotin-tagged SRC2-3 L*XX*LL motif to PPARγ.

RESULTS

PGC-1α LXXLL Motif Binding Affinity for PPARγ in Response to the Ligand Rosiglitazone—The recruitment of specific coactivators by PPARγ is the major factor that determines the transcriptional profile of target genes and the pharmacological actions of rosiglitazone (27, 28). To characterize the binding properties of various coactivators in response to rosiglitazone, we measured the direct interactions of purified PPARγ LBD with a panel of biotinylated peptide motifs from coactivators using AlphaScreen assays (26, 29). In this assay, the coactivator peptides and the PPARγ LBD protein were attached to donor and acceptor beads, respectively. Upon interaction between the coactivator peptides and the PPARγ LBD, excitation with a laser beam at 680 nm causes the donor beads to emit single oxygen molecules that activate fluorophores in the acceptor beads, and the light is recorded at 520–620 nm. As shown in Fig. 1*A*, the rosiglitazone-bound PPARγ LBD induced a strong interaction with various coactivator L*XX*LL motifs from the SRC family of coactivators, CBP, TRAP220, and the PGC-1α ID1 motif. These data are in agreement with the agonist property of rosiglitazone. Notably, even in the absence of rosiglitazone, PPARγ showed significant interactions with several coactivator motifs (particularly the PGC-1α ID1 motif), consistent with the high basal activation properties of PPARγ.

To determine which coactivators are preferentially recruited, we performed a peptide profiling experiment using a panel of unlabeled peptides to compete off the binding of the biotinylated third L*XX*LL motif of SRC2 (SRC2-3) to the rosiglitazone-bound PPARγ LBD (Fig. 1*B*). In this experiment, all unlabeled peptides were applied at a uniform concentration of 500 nM under identical experimental conditions. Thus the relative binding affinity of individual peptides to PPARγ LBD can be measured by the degree of its inhibition of the binding of the biotinylated SRC2-3 motif to the PPARγ LBD. In the absence of any competing peptides, interaction between the biotinylated SRC2-3 motif and the PPARγ LBD yielded a count of 27,000 photons (Fig. 1*B*). Most unlabeled peptide motifs gave little competition to coactivator binding of PPARγ at a concentration of 500 nM; the PGC-1α ID1 motif showed the most significant competition.

The high binding affinity of PPARγ toward the PGC-1α ID1 motif was further determined by IC_{50} values from quantitative competition experiments using unlabeled peptides (Fig. 2). Consistent with the peptide profiling, PPARγ bound to the PGC-1α ID1 motif with higher affinity than to ID2 (IC_{50} of 1.7 μM *versus* 87 μM) (Fig. 2*A*). Relative to the IC_{50} of L*XX*LL motifs from SRC families, the PGC-1α ID1 motif also displayed stronger binding affinity to PPARγ (Fig. 2*B*). Interestingly, rosiglitazone increased the binding affinity of PPARγ with most coactivator motifs tested. The remarkable selectivity of PPARγ toward PGC-1α is consistent with the fact that PGC-1α is a well established coactivator for PPARγ in adipogenesis and glucose metabolism (30). Together, these results demonstrate that rosiglitazone promotes the interaction of coactivator motifs with PPARγ and that PGC-1α ID1 preferentially binds to PPARγ with the highest affinity among all coregulator motifs tested.

Structure of the PPARγ LBD·Rosiglitazone·PGC-1α Complex—Because the first L*XX*LL motif of PGC-1α (ID1) binds to PPARγ with the highest affinity, we wanted to know the molecular mechanism underlying the binding selectivity of PPARγ

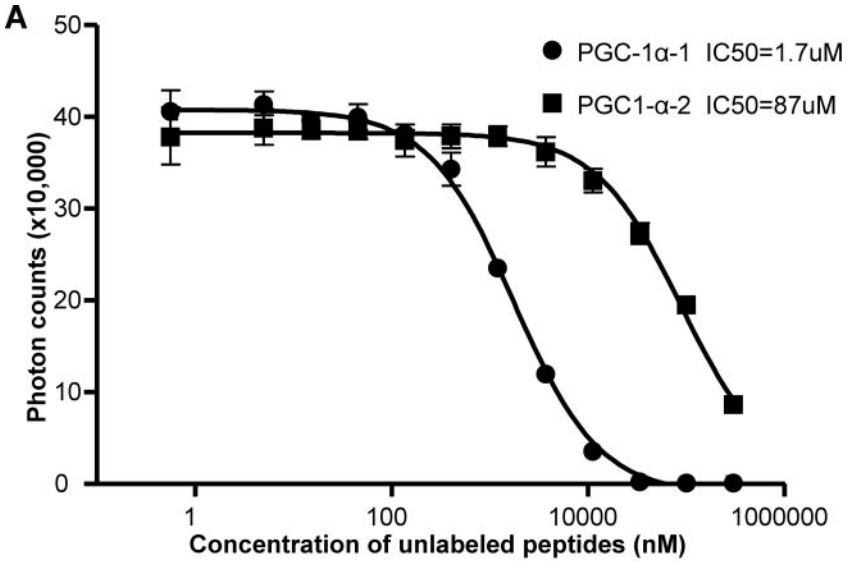

B

Peptides	------ LXXLL ----	Apo IC50 (μM)	Rosiglitazone (μM)
PGC1-α-1:	AEEPSL LKKLL LAPA	3.7±0.5	1.7±0.2
PGC1-α-2:	RRPCSE LLKYL TTND	43±9	87±20
SRC1-2:	TERHKI LHRLL QESS	40±7.9	42.3±3.6
SRC1-3:	SKDHQL LRYLL DKDE	>400	108±26
SRC1-4:	AQQKSL LQQLL TE	111±26	31.9±6
SRC2-2:	KEKHKI LHRLL QDSS	173±57	153±39
SRC2-3:	KENAL LRYLL DKDD	262±100	57.7±9.8
SRC3-1:	SKGHKK LLQLL TCSS	>400	38.5±5.5
SRC3-2:	QEKHRI LHKLL QNGN	57.7±13	16.3±1.8
SRC3-3:	KENNAL LRYLL DRDD	>400	98±25

FIGURE 2. **Binding affinity of various PGC-1α and SRC L*XX*LL motifs to the purified PPARγ LBD as determined by IC_{50} values from peptide competition experiments using AlphaScreen assays.** *A*, dose-response curves of the PPARγ LBD to the ID1 and ID2 motifs of PGC-1α in the presence of rosiglitazone ligand. *B*, the IC_{50} values of various PGC-1α and SRC L*XX*LL motifs to the purified PPARγ LBD in the absence (*Apo*) and presence of rosiglitazone. The numbering scheme of the L*XX*LL motifs is shown on the top of the sequences.

toward PGC-1α. To determine the roles of the two receptor-interacting motifs (ID1 and ID2) of PGC-1α in binding to PPARγ, we purified a PGC-1α fragment (residues 101–220) containing both ID1 and ID2 interacting motifs and complexed it with the PPARγ LBD for crystallization studies (Fig. 3*A*). The PPARγ LBD and the PGC-1α fragment were purified individually, mixed to form the complex with PGC-1α in excess, and then further purified through a gel filtration column (Fig. 3, *B* and *C*). In the gel filtration profile, the PGC-1α·PPARγ complex is shifted left because of its greater size, whereas PGC-1α alone eluted out in the volume of smaller size. We collected and concentrated the complex peak to a final concentration of 10 mg/ml for crystallization trials, and PPARγ·rosiglitazone·PGC-1α crystals were readily obtained at room temperature (Fig. 3*D*).

The PPARγ·rosiglitazone·PGC-1α complex crystallized in the C2 space group with one complex in each asymmetric unit. The structure was solved by molecular replacement using the structure of the PPARγ LBD bound to rosiglitazone and the SRC1-2 motif as the initial model (21). The calculated electron density map using the initial molecular replacement solution showed clear features of the PPARγ LBD, the bound ligand rosiglitazone, and a single PGC-1α L*XX*LL motif. Although a large PGC-1α fragment (120 amino acids) was used in crystallization, most sequences except the ID1 motif are invisible because of very low and ambiguous electron density. The statistics of data and the refined structure are listed in Table 1.

The overall structure of the PPARγ·rosiglitazone·PGC-1α complex is shown in Fig. 4*A*. Specifically, the PPARγ LBD is composed of 13 α helices and four short β strands that are folded into a three-layer helical sandwich. The C-terminal activation function 2 helix is positioned in the active conformation by packing tightly against the main domain of the LBD. In this conformation, the activation function 2 helix, together with helices H3, H4, and H5, forms a charge-clamp pocket where the PGC-1α L*XX*LL motif is docked.

Functional Interaction of PGC-1α and PPARγ through the PGC-1α ID1 Motif—Despite both the ID1 and ID2 motifs being in the PGC-1α fragment used for crystallization, the structure of the PPARγ LBD·PGC-1α complex shows that only the ID1 motif is bound in the coactivator binding site. The LKKLL sequence of the PGC-1α ID1 motif can be clearly identified by the distinguishing features of the electron density map, where the core LKKLL motif adopts a two-turn α helix with its hydrophobic leucine side chains directed toward the hydrophobic surface of the coactivator binding groove of PPARγ (Fig. 4, *B* and *C*). The overall structure of the PPARγ coactivator binding site and the docking mode of PGC-1α ID1 resemble those observed in other nuclear receptor coactivator complexes (9). Beside the core LKKLL motifs, several flanking residues are also clearly visible in the electron density map (Fig. 4*B*). Thus, the structure of the PPARγ LBD·PGC-1α complex and the biochemical AlphaScreen results both indicate that the binding of PGC-1α to PPARγ is through the PGC-1α ID1 L*XX*LL motif.

To further establish the role of PGC-1α ID1 and ID2 in binding to PPARγ, we performed mammalian two-hybrid assays using the PGC-1α fragment that contains both these motifs. The PGC-1α fragment was fused with the Gal4 DNA-binding domain, and the PPARγ LBD was fused with the VP16 activation domain (Fig. 4, *D* and *E*). We mutated individual L*XX*LL motifs of PGC-1α to A*XX*LA, resulting in PGC-1αM1 and

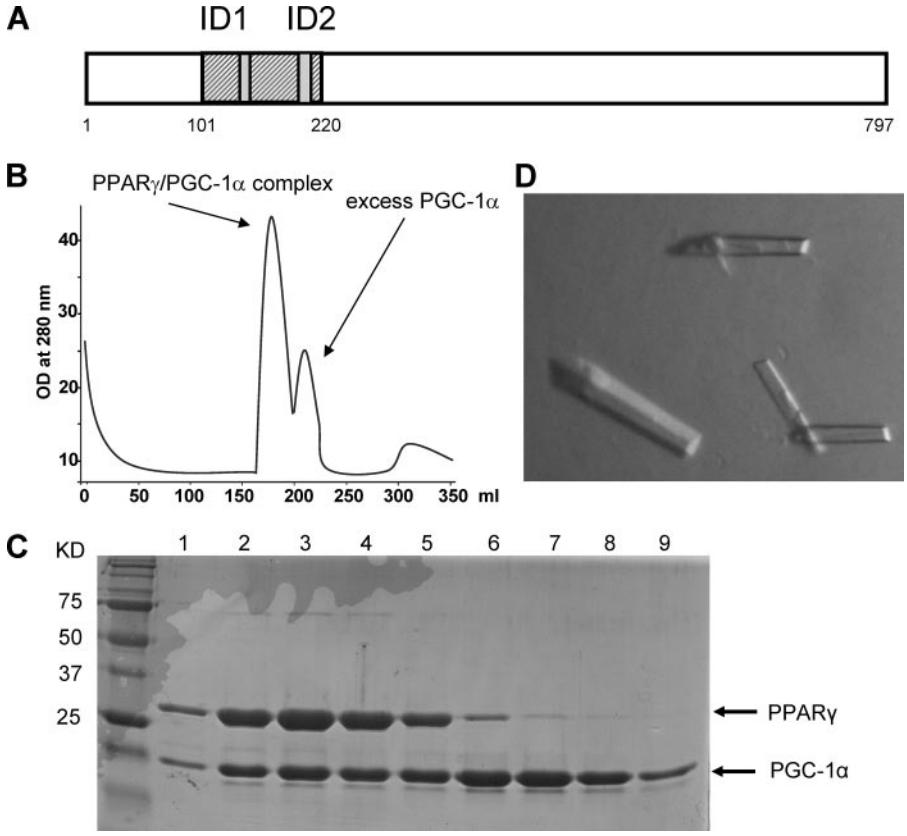

FIGURE 3. **Purification and crystallization of the PPARγ LBD complexed with a PGC-1α fragment.** *A*, a schematic representation showing the PGC-1α protein and its two receptor-interacting motifs (ID1 and ID2). The PGC-1α fragment (101–220) that includes both ID1 and ID2 motifs was used in cocrystallization with PPARγ. *B*, purification of the PPARγ LBD and PGC-1α complex. The proteins of PPARγ and PGC-1α were purified separately and complexed using excess PGC-1α in the presence of rosiglitazone. The PPARγ·PGC-1α complex and PGC-1α alone were separated by gel filtration. The complex was eluted in the first peak and collected and concentrated to 10 mg/ml for the crystallization trial. *C*, the protein complex samples shown on an SDS gel. The molecular mass markers are shown in the *KD lane* (kilodaltons). *Lanes 1–9* are fractions from the gel filtration column corresponding to the two peaks in *B*, from *left* to *right*. *D*, crystals of the PPARγ·rosiglitazone·PGC-1α complex.

TABLE 1
Statistics of data and structure

	PPARγ·PGC-1α complex
Crystal data	
X-ray source	APS-32ID
Space group	C2
Resolution (Å)	50.0-2.30
Unique reflections	15,354
Completeness (%)	100
I/σ	10.95
R_{sym} (%)[a]	15.5
Mosaicity	0.51
Refinement statistics	
R factor (%)[b]	24.84
R_{free} (%)	27.45
r.m.s.d.[c]	
Bond lengths (Å)	0.01
r.m.s.d. bond	
Angles	1.70°
Total non-hydrogen atoms	2515

[a] $R_{sym} = \Sigma|I_{avg} - I_i|/\Sigma I_i$.
[b] R factor $= \Sigma|F_p - F_{p(calc)}|/\Sigma F_p$, where F_p and $F_{p(calc)}$ are the observed and calculated structure factors, respectively; R_{free} was calculated from a randomly chosen 8% of reflections excluded from refinement; and R factor was calculated for the remaining 92% of the reflections.
[c] r.m.s.d., root mean square deviation from the ideal geometry of protein.

PGC-1αM2, and tested the ability of these mutated coactivators to potentiate the PPARγ-mediated activation in response to rosiglitazone. Mutations in the ID2 motif of PGC-1α decreased the interaction with PPARγ, whereas the activation in response to rosiglitazone remained unchanged (Fig. 4*D*). However, mutation of the ID1 motif completely abolished the ability of PGC-1α to bind PPARγ, consistent with the dominant role of ID1 in binding to PPARγ as revealed by the structure and the AlphaScreen assays.

PGC-1α is also able to coactivate a number of other nuclear receptors, including ERRα, a constitutively active receptor. To compare PGC-1α interactions between PPARγ and ERRα, we performed similar mammalian two-hybrid experiments on PGC-1α and ERRα. As expected, ERRα interacts with PGC-1α in the absence of any ligand treatment, consistent with the high constitutive activity of ERRα (Fig. 4*E*). In contrast to PPARγ, mutations in the ID1 or ID2 motifs of PGC-1α both substantially reduced ERRα-PGC-1α interactions. These results suggest that PGC-1α uses different interacting domains (ID1 or ID2) in its preferential binding to various nuclear receptors: PPARγ prefers ID1, and ERRα requires both ID1 and ID2.

To further determine the functional significance of PGC-1α ID1 in the ligand-regulated activity of PPARγ, we mutated either the ID1 or ID2 motifs of PGC-1α within the context of the full-length PGC-1α coactivator and tested the effect of these mutated coactivators on PPARγ-mediated activation in cell-based assays (Fig. 5). The plasmid encoding full-length PPARγ and a PPARγ response reporter were transiently cotransfected into cells, and the assays were performed in the presence or absence of rosiglitazone. Fig. 5 shows that wild-type PGC-1α substantially elevates the transcriptional activity of PPARγ with or without rosiglitazone. Although no effect on reporter activity was observed upon cotransfection with the PGC-1α ID2 mutant, the mutation in the ID1 motif completely abolished the ability of PGC-1α to coactivate PPARγ-mediated transcription. These results further demonstrate the functional significance of the PGC-1α ID1 in binding to PPARγ and highlight a crucial role of the PGC-1α ID1 motif in the coactivation of PPARγ.

Molecular Determinants for the Preferential Recruitment of PGC-1α by PPARγ—The PPARγ LBD·PGC-1α structure is the first structure of a nuclear receptor with the PGC-1α ID1 motif, and it reveals a molecular basis for the preferential binding of this motif to the PPARγ receptor. In addition to the hydrophobic interactions with PPARγ by its core L*XX*LL motif, which is conserved for the binding of nuclear receptors (Fig. 6*A*),

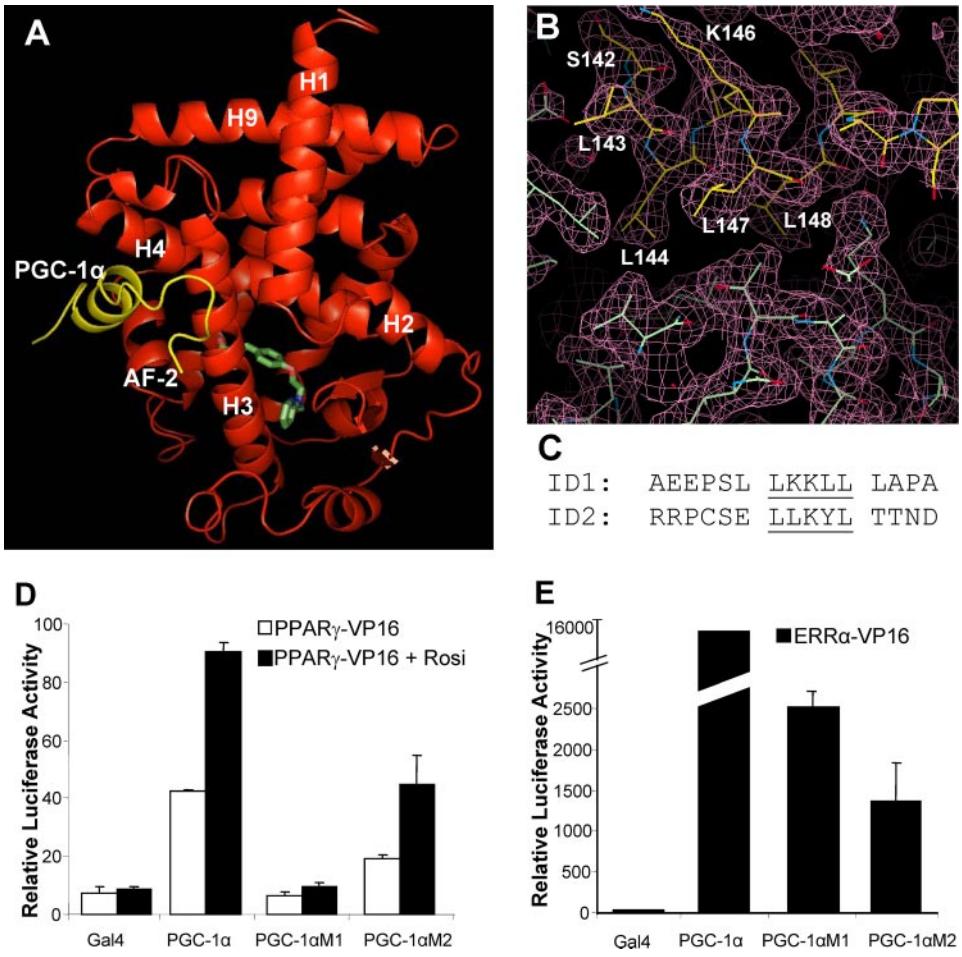

FIGURE 4. **The binding of PGC-1α to PPARγ is through the PGC-1α ID1 L*XX*LL motif.** *A*, the overall structure of the PPARγ·rosiglitazone·PGC-1α complex in ribbon representation. PPARγ is *red*, the PGC-1α is in *yellow*, and the bound rosiglitazone is shown in stick representation with carbon and oxygen atoms depicted in *green* and *red*, respectively. *B*, a $2F_o - F_c$ electron density map (1.0 σ) showing the binding interface of PPARγ and PGC-1α. *C*, an alignment of core sequences of PGC-1α ID1 and ID2. *D* and *E*, the roles of PGC-1α ID1 and ID2 in the interaction with PPARγ and ERRα. Mammalian two-hybrid assays were performed in COS-7 cells. The PGC-1α fragment that contains both ID1 and ID2 was fused to the Gal4 DNA-binding domain, and the LBDs of ERRα and PPARγ were fused with VP16 AD. The ligand-dependent interaction of PPARγ with PGC-1α was analyzed using 1 μM rosiglitazone (*Rosi*).

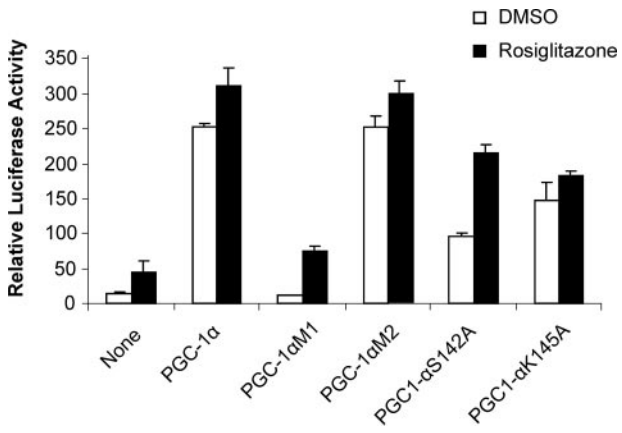

FIGURE 5. **Functional correlation of the PGC-1α/PPARγ interactions and the effects of PGC-1α mutations on the coactivation of PPARγ.** The cells were cotransfected with the PPRE luciferase reporter, together with plasmids encoding full-length PPARγ and full-length PGC-1α (wild type or mutants as indicated in the figure). *DMSO*, dimethyl sulfoxide.

PGC-1α contains two unique features within the structure that define its high affinity binding to PPARγ (Fig. 6, *B–D*). The first feature is that Lys[145] in the core region of PGC-1α ID1 forms a direct hydrogen bond with Asn[312] in PPARγ (Fig. 6, *B* and *C*). This hydrogen bond stabilizes the binding of PPARγ and PGC-1α in addition to the hydrophobic interactions between these two molecules. The second feature is the remarkable stability of the PGC-1α ID1 helix through its intramolecular interactions. In the structure, Ser[142] forms a direct hydrogen bond that caps the backbone amide of Glu[140] of the L*XX*LL helix (Fig. 6*D*). These intramolecular interactions are likely to stabilize the overall helical structure of the PGC-1α ID1 motif, thus facilitating the hydrophobic docking of this helix into PPARγ. Together, these unique intermolecular and intramolecular contacts serve as a basis for the high affinity and specific binding of PPARγ toward PGC-1α.

To assess the importance of these interactions in the PGC-1α-mediated enhancement of PPARγ activity, we made the mutations S142A and K145A in PGC-1α ID1 and tested these mutants in cell-based assays using full-length PPARγ and a PPARγ response reporter (Fig. 5). In the absence of ligand, the S142A mutation substantially reduced PGC-1α-mediated coactivation of PPARγ. PGC-1α-mediated coactivation was also impaired by this mutation in the presence of rosiglitazone. Similar results were also observed for the K145A mutant, suggesting that both Ser[142] and Lys[145] of PGC-1α contribute to its ability to coactivate PPARγ. Together, these results reveal that the strong interaction of PGC-1α with PPARγ is due to hydrophobic binding of its ID1 L*XX*LL motif and also to specific interactions between the two molecules.

DISCUSSION

As a master regulator of adipose differentiation, PPARγ serves as a key transcriptional factor that links obesity, diabetes, and cardiovascular diseases through selective recruitment of various coregulatory proteins with distinct functions. The various transcriptional coactivators display many distinct physiological roles, such as enzymatic activities like histone acetylation and deacetylation. For instance, SRC1 and SRC2 (also known as GRIP1/TIF2) have been shown to play opposite roles

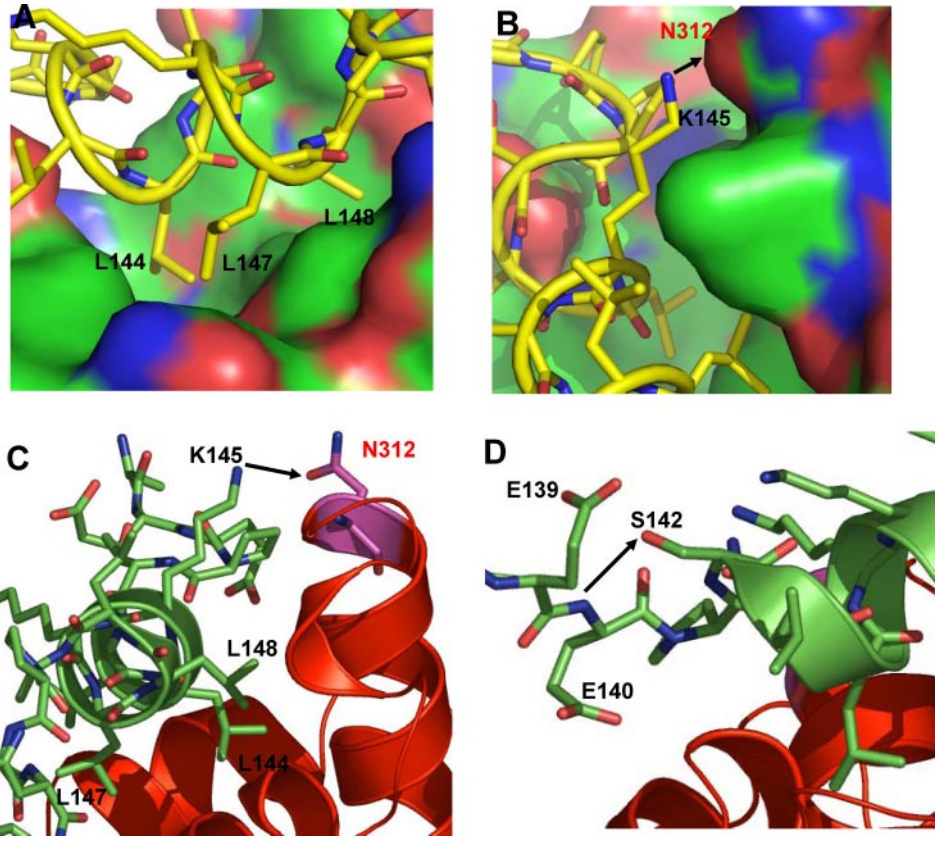

FIGURE 6. **Molecular determinants of the PGC-1α/PPARγ interactions.** *A* and *B*, the docking mode of PGC-1α ID1 (*yellow*) on the surface of PPARγ (coactivator binding site) is shown. The hydrophobic interaction is shown in *A*, and the specific intermolecular interaction is shown in *B*. *C* and *D*, the binding interface of PGC-1α/PPARγ shows the specific intermolecular and intramolecular interactions. The PGC-1α is shown in *green*, the PPARγ is in *red*, and the hydrogen bonds are shown as *arrows*.

in energy metabolism in mouse knock-out studies (31). SRC1$^{-/-}$ mice are prone to obesity because of reduced energy expenditure, whereas SRC2$^{-/-}$ mice are protected against obesity and display enhanced adaptive thermogenesis. Accordingly, *N*-(9-fluorenyl)methoxycarbonyl (Fmoc)-L-leucine, a distinct PPARγ ligand, preferentially recruits SRC1 (but not SRC2) by inducing a particular allosteric configuration of the PPARγ coregulator binding interface (32). As a result, this unique ligand enhances insulin sensitivity and reduces glucose levels without promoting the weight gain normally associated with the thiazolidinedione class of PPARγ ligands. Thus, the selective modulation of PPARγ activity is highly dependent on its ability to recruit specific coactivators.

Here we conducted detailed analysis of the interplay between rosiglitazone-regulated PPARγ and coactivators through a combination of mutagenesis, biochemical binding profiling, and structural analysis. Our quantitative competition experiments show that rosiglitazone-bound PPARγ has a marked binding preference for the PGC-1α ID1 motif (Figs. 1 and 2). Consistent with this result, the crystal structure of the PPARγ·PGC-1α complex reveals the docking mode of the PGC-1α ID1 helix (Fig. 4, *A* and *B*). Our mutagenesis studies further demonstrate the essential roles of the ID1 motif in the functional interaction between PGC-1α and PPARγ (Figs. 4*D* and 5). Interestingly, increased expression of PGC-1α has been shown in rosiglitazone treatment (18, 27). The coexpression of PGC-1α and PPARγ in rosiglitazone target tissues and the strong interaction between them suggest the importance of the interaction of PPARγ and PGC-1α in the pharmacological roles of rosiglitazone.

The molecular basis for the selective binding of PPARγ with PGC-1α is provided by the structure of the bound pair. This structure reveals specific intermolecular and intramolecular interactions that define the preferential binding between rosiglitazone-bound PPARγ and PGC-1α (Fig. 6). Mutations designed to disrupt these interactions reduce the binding of PGC-1α to PPARγ in cell-based transcriptional assays (Fig. 5). In addition, we have demonstrated that different receptors can differ in their interaction with PGC-1α by using alternative interaction sites. Although ID2 is not required for PGC-1α interaction with PPARγ, this motif is shown to bind to the nuclear receptor ERRα (15, 19). Interestingly, ID2 contains an atypical L*XX*YL motif, which is an inverted L*XX*LL sequence. Instead of three hydrophobic leucine side chains, ID2 uses two leucine side chains to dock into the groove of the ERRα coactivator binding site. The interaction is further strengthened by the favorable van der Waals contacts between the tyrosine in the PGC-1α ID2 core and ERRα residues Leu^{333}, Ile^{336}, and Leu^{509} (19). However, these ERRα residues are not conserved in PPARγ, and the coregulator binding interface of PPARγ shows binding properties distinct from those of ERRα. As such, only PGC-1α ID1 is capable of strong binding to PPARγ, whereas PGC-1α ID2 has a much lower affinity. Structural comparison between the PPARγ·PGC-1α ID1 and ERRα·PGC-1α ID2 complexes shows that these two nuclear receptors employ distinct structural mechanisms to achieve specific recognition of their coactivators. As PGC-1α also strongly interacts with PPARα, PPARβ/δ, and a large number of other nuclear receptors, the structure of the PPARγ·PGC-1α complex will have broad implications for understanding PGC-1α receptor interactions.

Acknowledgments—We thank D. Nadziejka for professional editing of the manuscript; B. M. Spiegelman, A. Kralli, and Eugene Chen for cDNAs of various receptors and reporter plasmids; and W. D. Tolbert and J. S. Brunzelle for assistance in data collection at sector 32 of the Advanced Photon Source.

REFERENCES

1. Lehrke, M., and Lazar, M. A. (2005) *Cell* **123,** 993–999
2. Feige, J. N., Gelman, L., Michalik, L., Desvergne, B., and Wahli, W. (2006) *Prog. Lipid Res.* **45,** 120–159

3. Glass, C. K., and Ogawa, S. (2006) *Nat. Rev. Immunol.* **6,** 44–55
4. Girnun, G. D., Naseri, E., Vafai, S. B., Qu, L., Szwaya, J. D., Bronson, R., Alberta, J. A., and Spiegelman, B. M. (2007) *Cancer Cell* **11,** 395–406
5. Hall, J. M., and McDonnell, D. P. (2007) *Mol. Endocrinol.* **21,** 1756–1768
6. Nissen, S. E., and Wolski, K. (2007) *N. Engl. J. Med.* **356,** 2457–2471
7. Lonard, D. M., and O'Malley, B. W. (2007) *Mol. Cell* **27,** 691–700
8. Lonard, D. M., Lanz, R. B., and O'Malley, B. W. (2007) *Endocr. Rev.* **28,** 575–587
9. Li, Y., Lambert, M. H., and Xu, H. E. (2003) *Structure* (*Camb.*) **11,** 741–746
10. Nettles, K. W., Sun, J., Radek, J. T., Sheng, S., Rodriguez, A. L., Katzenellenbogen, J. A., Katzenellenbogen, B. S., and Greene, G. L. (2004) *Mol. Cell* **13,** 317–327
11. Puigserver, P., Wu, Z., Park, C. W., Graves, R., Wright, M., and Spiegelman, B. M. (1998) *Cell* **92,** 829–839
12. Knutti, D., Kaul, A., and Kralli, A. (2000) *Mol. Cell. Biol.* **20,** 2411–2422
13. Vega, R. B., Huss, J. M., and Kelly, D. P. (2000) *Mol. Cell. Biol.* **20,** 1868–1876
14. Tcherepanova, I., Puigserver, P., Norris, J. D., Spiegelman, B. M., and McDonnell, D. P. (2000) *J. Biol. Chem.* **275,** 16302–16308
15. Huss, J. M., Kopp, R. P., and Kelly, D. P. (2002) *J. Biol. Chem.* **277,** 40265–40274
16. Wu, Y., Chin, W. W., Wang, Y., and Burris, T. P. (2003) *J. Biol. Chem.* **278,** 8637–8644
17. Lin, J., Handschin, C., and Spiegelman, B. M. (2005) *Cell Metab.* **1,** 361–370
18. Wilson-Fritch, L., Nicoloro, S., Chouinard, M., Lazar, M. A., Chui, P. C., Leszyk, J., Straubhaar, J., Czech, M. P., and Corvera, S. (2004) *J. Clin. Investig.* **114,** 1281–1289
19. Kallen, J., Schlaeppi, J. M., Bitsch, F., Filipuzzi, I., Schilb, A., Riou, V., Graham, A., Strauss, A., Geiser, M., and Fournier, B. (2004) *J. Biol. Chem.* **279,** 49330–49337
20. Otwinowski, Z., and Minor, W. (1997) *Methods Enzymol.* **276,** 307–326
21. Gampe, R. T., Jr., Montana, V. G., Lambert, M. H., Miller, A. B., Bledsoe, R. K., Milburn, M. V., Kliewer, S. A., Willson, T. M., and Xu, H. E. (2000) *Mol. Cell* **5,** 545–555
22. Navaza, J., Gover, S., and Wolf, W. (1992) in *Molecular Replacement: Proceedings of the CCP4 Study Weekend* (Dodson, E. J., ed) SERC, Daresbury, UK
23. Brunger, A. T., Adams, P. D., Clore, G. M., DeLano, W. L., Gros, P., Grosse-Kunstleve, R. W., Jiang, J. S., Kuszewski, J., Nilges, M., Pannu, N. S., Read, R. J., Rice, L. M., Simonson, T., and Warren, G. L. (1998) *Acta Crystallogr.* **54,** 905–921
24. Xu, H. E., Stanley, T. B., Montana, V. G., Lambert, M. H., Shearer, B. G., Cobb, J. E., McKee, D. D., Galardi, C. M., Plunket, K. D., Nolte, R. T., Parks, D. J., Moore, J. T., Kliewer, S. A., Willson, T. M., and Stimmel, J. B. (2002) *Nature* **415,** 813–817
25. Suino, K., Peng, L., Reynolds, R., Li, Y., Cha, J. Y., Repa, J. J., Kliewer, S. A., and Xu, H. E. (2004) *Mol. Cell* **16,** 893–905
26. Li, Y., Suino, K., Daugherty, J., and Xu, H. E. (2005) *Mol. Cell* **19,** 367–380
27. Guan, H. P., Ishizuka, T., Chui, P. C., Lehrke, M., and Lazar, M. A. (2005) *Genes Dev.* **19,** 453–461
28. Yu, S., and Reddy, J. K. (2007) *Biochim. Biophys. Acta* **1771,** 936–951
29. Li, Y., Choi, M., Cavey, G., Daugherty, J., Suino, K., Kovach, A., Bingham, N. C., Kliewer, S. A., and Xu, H. E. (2005) *Mol. Cell* **17,** 491–502
30. Puigserver, P., and Spiegelman, B. M. (2003) *Endocr. Rev.* **24,** 78–90
31. Picard, F., Gehin, M., Annicotte, J., Rocchi, S., Champy, M. F., O'Malley, B. W., Chambon, P., and Auwerx, J. (2002) *Cell* **111,** 931–941
32. Rocchi, S., Picard, F., Vamecq, J., Gelman, L., Potier, N., Zeyer, D., Dubuquoy, L., Bac, P., Champy, M. F., Plunket, K. D., Leesnitzer, L. M., Blanchard, S. G., Desreumaux, P., Moras, D., Renaud, J. P., and Auwerx, J. (2001) *Mol. Cell* **8,** 737–747